Thermal-Error Regime in High-Accuracy Gigahertz Single-Electron Pumping

R. Zhao,[1,*] A. Rossi,[2] S. P. Giblin,[3] J. D. Fletcher,[3] F. E. Hudson,[1] M. Möttönen,[4] M. Kataoka,[3] and A. S. Dzurak[1]

[1]*School of Electrical Engineering and Telecommunications, University of New South Wales, Sydney, New South Wales 2052, Australia*

[2]*Cavendish Laboratory, University of Cambridge, J J Thomson Avenue, Cambridge CB3 0HE, United Kingdom*

[3]*National Physical Laboratory, Hampton Road, Teddington, Middlesex TW11 0LW, United Kingdom*

[4]*QCD Labs, COMP Centre of Excellence, Department of Applied Physics, Aalto University, 00076 Aalto, Finland*

(Received 21 March 2017; revised manuscript received 13 September 2017; published 30 October 2017)

Single-electron pumps based on semiconductor quantum dots are promising candidates for the emerging quantum standard of electrical current. They can transfer discrete charges with part-per-million (ppm) precision in nanosecond time scales. Here, we employ a metal-oxide-semiconductor silicon quantum dot to experimentally demonstrate high-accuracy gigahertz single-electron pumping in the regime where the number of electrons trapped in the dot is determined by the thermal distribution in the reservoir leads. In a measurement with traceability to primary voltage and resistance standards, the averaged pump current over the quantized plateau, driven by a 1-GHz sinusoidal wave in the absence of a magnetic field, is equal to the ideal value of ef within a measurement uncertainty as low as 0.27 ppm.

DOI: 10.1103/PhysRevApplied.8.044021

I. INTRODUCTION

Single-electron (SE) pumps can generate quantized electrical current by controlling the transport of individual electrons with an external periodic drive [1,2]. These devices relate the pumped direct current I to the elementary charge e and the driving frequency f through the expression $I = nef$, where n is an integer. As an on-demand SE source, they can be useful in the context of quantum information processing as well as in the study of fermionic optics [3–5]. Arguably, the most important application of this technology is to realize a quantum standard of electrical current [6].

Single-electron pumps and turnstiles have been realized in various physical systems, including normal-metal tunnel-junction devices [7,8], surface acoustic-wave devices [9,10], superconducting devices [11–13], hybrid superconductor-normal-metal turnstiles [14], quantum dots [15–27], and single dopants or traps [28–32]. The tunable-barrier SE pumps based on semiconductor quantum dots (QDs) stand out from the competing technologies for providing a good balance between low pumping error and high output current [17,25,27,33,34].

Three different designs of GaAs pumps have achieved relative errors close to or below 1 part per million (ppm) in high-accuracy measurements traceable to primary standards [17,18,33–35]. These GaAs pumps transport a fixed number of electrons per cycle following a series of sequential back-tunneling events, known as the decay cascade [36]. Previous studies indicate that strong magnetic fields, tailored waveform drives, and subkelvin temperatures are required for the GaAs pumps to achieve ppm-level accuracy at gigahertz pumping frequencies [17,33,34]. These requirements render the realization of the quantum current standard demanding and restrict the user base of GaAs pump technology.

In contrast, QD pumps in silicon alleviate some of these burdens. Compared to depletion mode GaAs QDs, the gate-voltage-induced silicon QDs tend to have a larger addition energy due to their smaller physical size. This feature of the compact silicon devices enables accurate high-frequency SE pumping in the decay-cascade regime without arbitrary waveform drives or high magnetic fields [25,27]. The remarkable results recently achieved in silicon devices not only demonstrate the universality of SE pumping in tunable-barrier QDs at sub-ppm uncertainty, but also clearly indicate that a compact silicon SE pump may pave the way towards a more practical quantum standard of electrical current [27]. From a pragmatic point of view, it is advantageous to implement the quantum current standard in silicon, since it is compatible with the metal-oxide-semiconductor (MOS) technology widely employed in industry. Through well-established fabrication techniques, silicon SE pumps can be seamlessly integrated with peripheral control circuits to deliver a cost-effective on-chip current standard.

One challenge for the SE pumps is that the large rf-drive amplitude usually required at gigahertz pumping frequency may heat the electron reservoir up to several kelvins and result in excessive thermal errors [24,37]. When the electron reservoir temperature increases, forward tunneling of thermally excited electrons from the reservoir into the

*ruichen.zhao@student.unsw.edu.au

QD becomes significant during the charge-capturing process, and the number of electrons trapped in the QD reflects the Fermi distribution of electrons in the leads [38,39]. To the best of our knowledge, gigahertz high-accuracy SE pumping in the thermal regime has not been achieved among the silicon devices.

In this work, we use a silicon QD, fabricated employing a MOS planar gate-stack technology [40,41], to demonstrate high-accuracy SE pumping in the regime where the number of pumped electrons in each cycle is determined by the thermal distribution of electrons in the reservoir leads. We investigate whether the accuracy of our SE pump significantly deteriorates due to drive-induced heating in the electron reservoir, as reported in previous studies [24,37]. Fits of the measurement data to the thermal model of electron capture yield a theoretical lower bound of 4 parts per billion (ppb) for the thermal error on the ef current plateau at $f = 1$ GHz. In addition, we experimentally measure the pumped current using a high-accuracy measurement setup, which compares the pumped current to a reference current derived from primary voltage and resistance standards [17]. We find that the averaged current on the plateau, induced by a sine-wave drive in the absence of a magnetic field, matches the ef value within the measurement uncertainty of ∼0.3 ppm. This is the most accurate measurement of the current from a silicon electron pump to date.

II. DEVICE ARCHITECTURE AND EXPERIMENTAL METHODS

The sample used in the experiments is fabricated on a high-purity near-intrinsic silicon wafer. We thermally grow 7-nm high-quality SiO_2 gate oxide on top of the substrate. Three layers of aluminum gate electrodes are lithographically defined on top of the gate oxide. Between each layer, the sample is heated up to 150 °C in air to form an aluminum-oxide coating on the electrode surface. This coating provides good electrical insulation between different metal layers [40,41].

A scanning-electron-microscope image of the aluminum gate stack of a device similar to the one used in the experiments is shown in Fig. 1(a). These metal gates, connected to programmable dc voltage sources through 200-Hz low-pass filters, can locally induce two-dimensional electron-gas (2DEG) channels or potential barriers at the Si/SiO_2 interface. By tuning the individual gate voltages, a quantum dot containing a few conduction electrons can be defined below the plunger gate (PL), as shown in Fig. 1(a). Electron reservoirs are accumulated below the source lead (SL) and the drain lead (DL), electrically connecting the quantum dot to the Ohmic contacts.

We optimize the pump performance using a normal-accuracy measurement setup shown in Fig. 1(a). The pumped current I_P is measured by a low-noise transimpedance amplifier (Femto DDPCA300) connected to the drain contact. The reference current source used in high-accuracy measurement is also connected to the drain, but it is switched off ($V = 0$) in the normal-accuracy measurement setup. We operate the SE pump with a sinusoidal excitation. As shown in Fig. 1(b), each pumping cycle begins with the rf drive lowering the potential barrier between the QD and the source reservoir and loading the QD with electrons. Then the rf drive raises the barrier to trap electrons and eject some or all of them to the drain reservoir. Gate $B1$ is driven by a microwave source (HP8341B) through a room-temperature bias tee followed by a 9-dB attenuator. The source is synchronized to a 10-MHz reference frequency derived from a primary cesium frequency standard. All rf power levels quoted in

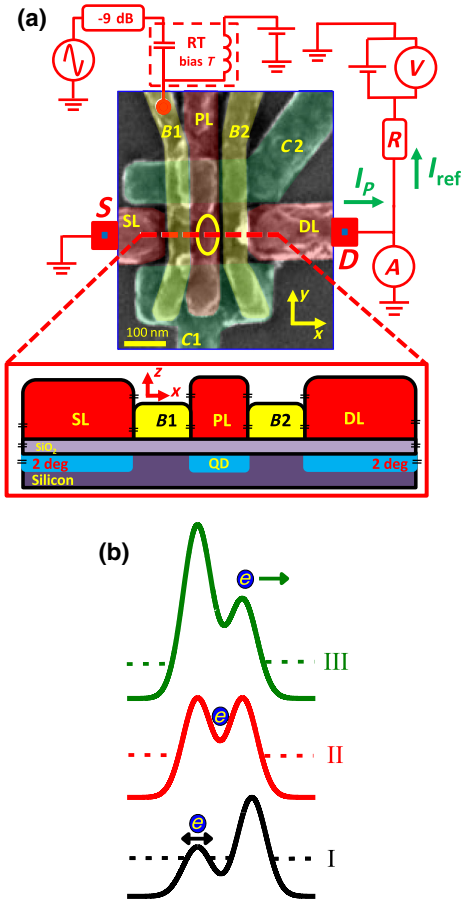

FIG. 1. (a) False-color scanning-electron-microscope image of an electron pump similar to the one used. The yellow circle highlights the approximate region where a quantum dot is formed. A schematic of the measurement setup as well as an illustrative cross-sectional view of the metal-oxide-semiconductor structure are also shown. The drain contact is connected to the reference current source used in the high-accuracy measurements. It consists of a temperature-controlled 1-GΩ-thick film resistor and a voltage source (Keithley213) monitored by a high-accuracy voltmeter (HP 3458A). (b) Sketch of the conduction-band energy profile (solid lines) and Fermi level (dashed lines) during a pumping cycle.

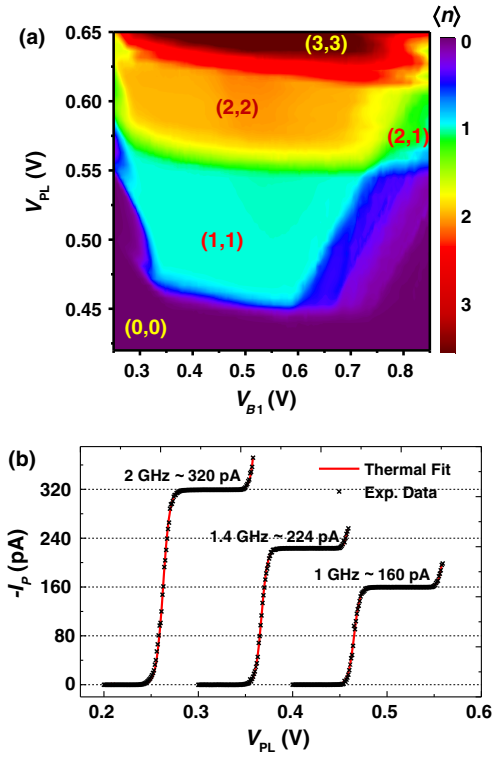

FIG. 2. (a) Coarsely tuned current plateaus at $f = 500$ MHz measured using the normal-accuracy setup. In the notation (m, n), m (n) represents the ideal number of captured (ejected) electrons. Here, $V_{SL} = V_{B2} = 1.5$ V, $V_{DL} = 1.75$ V, $V_{C1} = -1$ V, $V_{C2} = 0.2$ V, and $P_{B1} = 2$ dBm. (b) Normal-accuracy measurements (black crosses) of pumped current as a function of the plunger gate voltage for different pumping frequencies and fits to the thermal model (red solid lines). Data have been horizontally shifted for clarity. Parameter settings: $V_{SL} = V_{B2} = 1.5$ V, $V_{B1} = 0.45$ V, $V_{DL} = 1.9$ V, $V_{C1} = -1.04$ V, $V_{C2} = 0.187$ V, and $P_{B1} = 3$ dBm.

this paper refer to the power after the 9-dB attenuator. All measurements presented in this work are carried out on a single device in the absence of a magnetic field with a small ($\sim$250 μV) stray bias across the pump due to the current preamplifier. The sample is cooled in a helium-3 cryostat with a base temperature of 300 mK.

We take the following approach to search for a stable low-error current plateau: First, the capacitive coupling strength of the quantum dot to each gate is obtained from the period of the corresponding Coulomb blockade oscillations. Second, the two gate voltages that have the strongest capacitive coupling to the dot potential, namely, V_{B1} and V_{PL}, are selected to be the main sweep parameters. Third, a sinusoidal excitation with a relatively low frequency, starting from 500 MHz, is applied to $B1$. We gradually increase the rf-drive power P_{B1} until a plateau structure, shown in Fig. 2(a), appears in the V_{B1}-V_{PL} plane. Finally, we decrease V_{C1} and V_{C2} to obtain a flatter current plateau [25]. We verify the robustness of the well-optimized current plateau at high pumping frequencies. As shown in Fig. 2(b), the ef current plateau is well pronounced up to 2 GHz without changing the gate voltages or rf power.

The search time is determined by the scan speed of the normal-accuracy measurement setup, which is limited by the 200-Hz low-pass filters connected between the dc voltage sources and the metal gates in this study. The tune-up process lasted a few hours and is performed only once during the whole measurement campaign. The fine-tuned current plateau, presented in Fig. 2(b), is stable throughout the high-accuracy measurement over a time period of a few weeks. Using this tune-up procedure, tens of devices with identical design have showed high-frequency current plateaus. Although these devices showed extremely low theoretical error rates and an excellent stability over time, due to the limited access to the high-accuracy measurement setup, this latest study is the only one where we could experimentally determine the pumping accuracy at the sub-ppm level.

III. RESULTS

A. SE Pumping in the thermal regime

The shape of the current staircase between two adjacent plateaus as a function of the QD depth-tuning gate V_{PL} [Fig. 2(b)] provides information about the process by which the QD is decoupled from the source lead. To date, the reported accurate semiconductor pumps [17,18,27,33,35] have operated in the decay-cascade regime [36], where the final number of electrons in the QD is determined by a one-way cascade of back-tunneling events [36]. Consequently, the average number of captured electrons $\langle m \rangle$ is characterized experimentally by an asymmetric staircase modeled using a double-exponential function of the QD depth-tuning gate voltage, which in our device is V_{PL},

$$\langle m \rangle = \sum_n \exp[-\exp(-aV_{PL} + \Delta_n)], \tag{1}$$

where a and Δ_n are fit parameters.

In this work, we consider the possibility that the electron reservoir is heated by the large-amplitude sinusoidal drive, leading to charge capture in the thermal regime. In this regime, electrons are exchanged between the dot and the leads during the initialization, so that the average number of captured electrons $\langle m \rangle$ follows the grand canonical distribution [37] and can be expressed as

$$\langle m \rangle = \sum_n 1/\{1 + \exp[E_{\text{add}}^{(n)}/(k_B T)]\}, \tag{2}$$

where k_B is the Boltzmann constant, T is the electron temperature of the source reservoir, and $E_{\text{add}}^{(n)}$ is the addition energy of the nth electron. We assume that the addition energy is approximately a linear function of V_{PL} within the small voltage range swept for pumping in the single-electron

regime. Therefore, Eq. (2) can be further expressed as a function of V_{PL}

$$\langle m\rangle = \sum_n 1/[1+\exp(A_n + B_n V_{\mathrm{PL}})], \tag{3}$$

where A_n and B_n are the fit parameters for the nth current plateau. Assuming the ejection error is negligible during pumping, the normalized current $-I_P/ef$ measures the average number of captured electrons. In this work, the normalized pumped current $-I_P/ef$ is used in the numerical fit of $\langle m\rangle$ for both decay-cascade and thermal models.

As shown in Fig. 3(a), the current staircase of our device is more accurately described by the thermal model than the decay-cascade model. The reduced χ^2 fit error for the thermal model, displayed in Fig. 3(b), is significantly lower than that for the decay-cascade model for all studied pumping frequencies. This strongly suggests our device is indeed operating in the thermal regime.

We estimate the reservoir electron temperature for the measurement in Fig. 3 using the following method: We extract the ratio of $E_{\mathrm{add}}/(k_B T)$ from the thermal fits presented in Fig. 3. Along with an addition energy of 17 meV, calculated based on a conduction-band profile simulated in the commercial semiconductor software package ISE-TCAD [42], we deduce the local electron temperature near the SE pump to be around 9 K at a $f = 1$ GHz. We need to estimate the addition energy using a simulation because the tunnel barriers are made completely opaque in the SE-pumping regime in order to prevent cotunneling errors [43], which prevents the direct observation of E_{add} in conductance measurements. More details on the TCAD simulation and the estimation of the QD addition energy are presented in the Supplemental Material [44].

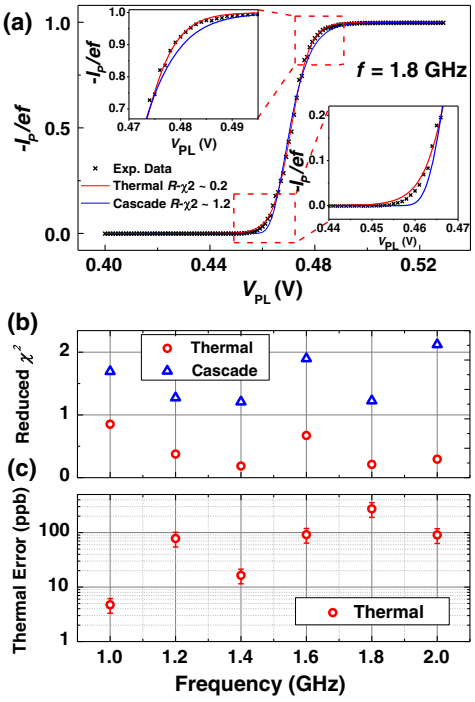

FIG. 3. (a) Normal-accuracy measurement (black crosses) of pumped current as a function of plunger gate voltage and its fits to the thermal (red solid line) and decay-cascade models (blue solid line). Insets: selected data from the main panel on expanded axes. (b) The reduced χ^2 fit error as a function of pumping frequency for both thermal and decay-cascade models. (c) The thermal error at the center of the first plateau predicted according to the fit to the thermal model at different frequencies. The plateau center is defined as the point of inflection of the thermal fit. The red error bar represents the typical error of the fit (~10%). For (a), (b), and (c), all gate-voltage settings and the rf power level are identical to Fig. 2(b).

In our previous work [25], a device with a similar design driven by a much smaller rf signal, roughly −6 dBm, demonstrated SE pumping in the decay-cascade regime. This suggests that the thermal regime observed in the present experiments is indeed due to heating of the electron reservoirs by the large rf-drive signal. A similar heating effect has been observed in a SE shuttle fabricated employing the same silicon technology [24]. An effective electron temperature of 7 K, attributed to rf-induced heating, has also been reported in another SE-pumping study employing a silicon nanowire device [37].

Next, we investigate whether the accuracy of our SE pump will, as reported in previous studies using silicon devices [24,37], significantly deteriorate due to such severe localized heating in the electron reservoir. Since our pump operated in the thermal regime, the main cause of the capture error is expected to be thermal fluctuations of the QD electron number during its decoupling from the source reservoir [37]. The thermal-error rate at the optimal working point of the $I = ef$ plateau can be estimated as $P_{\mathrm{error}}^{\mathrm{thermal}} = 1 - 1/\{1+\exp[E_{\mathrm{add}}^{(1)}/(k_B T)]\}$ [37], with the optimal working point given by the point of inflection of the fit line. Figure 3(c) shows the thermal-error rate as a function of frequency. Despite the elevated electron temperature, we find the thermal error is as low as 4 ppb for $f = 1$ GHz. However, this should only be considered a lower bound for the overall error rate. Other error mechanisms, such as the nonadiabatic excitation of the captured electron [27,28,45,46] may be present and are not considered in the above analysis.

B. High-accuracy measurement

To experimentally investigate the quantized current accuracy, we employ the high-accuracy measurement scheme described in Ref. [17]. We compare the pumped current I_P to a reference current I_{ref}, with traceability to primary voltage and resistance standards. The transimpedance amplifier is used to measure the difference between these currents, I_{null}. Because it measures a very small signal, the drift in gain of the transimpedance amplifier, for example, due to temperature fluctuations, introduces only a small contribution to the overall uncertainty.

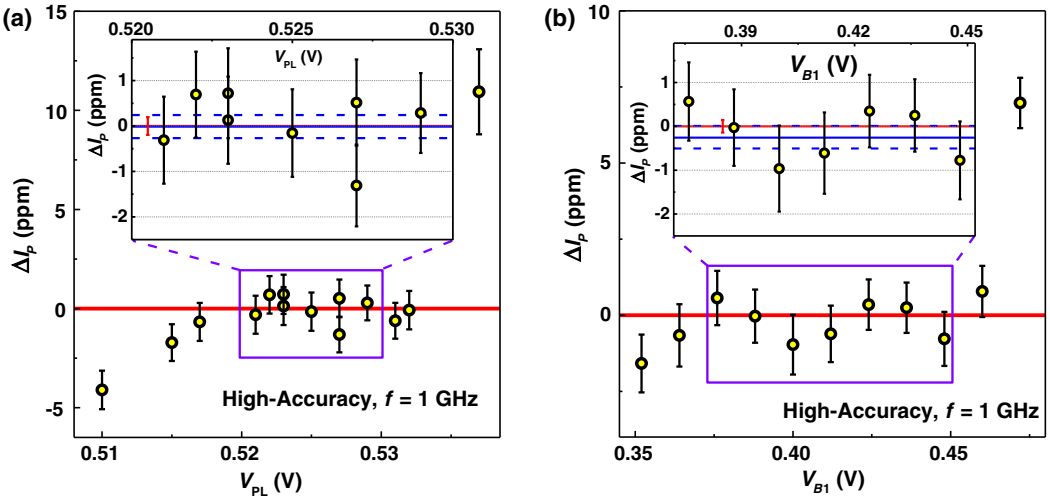

FIG. 4. High-accuracy measurements of the relative deviation ΔI_P of the pumped current I_P from the ideal ef value as functions of (a) V_{PL} and (b) V_{B1} at $f = 1$ GHz. Each data point is obtained by averaging 85 min of raw data. The black error bar represents the 1σ relative statistical uncertainty U_{ST} over each 85-min measurement, which is typically ~0.9 ppm. The red solid line indicates $\Delta I_P = 0$. We define the current plateau as the region where the fit to the thermal model deviates from ef by less than ± 0.03 ppm. Insets: Data points in the current plateau region on expanded axes. The red error bar corresponds to the relative systematic uncertainty for the measurement of I_{ref}. The blue solid (dashed) line corresponds to the mean (error of the mean) of the points on the plateau. All the uncertainties quoted in this paper are 1σ and have been rounded up to the next 0.01 ppm. The parameter settings are the same as in Fig. 2(b), except $V_{\mathrm{PL}} = 0.525$ V for (b).

In previous studies employing the same measurement setup [17,27,33], the 0.8-ppm systematic uncertainty in the calibration of the 1-GΩ resistor was by far the dominant contribution to the uncertainty budget. In this work, we introduce a revised uncertainty budget following a first-principles reevaluation of the cryogenic current comparator bridge used to calibrate the resistor [47]. In the revised uncertainty budget, the largest systematic term is 0.1 ppm, due to the 10-MΩ reference resistor used in the calibration, and the statistical uncertainty in the resistor calibration is also of the order of 0.1 ppm. A recent comparison of precision reference current sources [48] has highlighted problems with short-term drift affecting high-value standard resistors. To reduce the impact of this drift on the pump measurements to well below 0.1 ppm, in this work we calibrate the 1-GΩ resistor very frequently, with an interval between calibrations as short as two days.

We carry out our high-accuracy measurement on an optimized $I = ef$ plateau at 1 GHz. The pumped current as a function of V_{PL} is shown in Fig. 4(a), where the fractional deviation of the pumped current from ef is defined as $\Delta I_P \equiv (I_P - e_{90}f)/e_{90}f$. We use $e_{90} \equiv 2/(R_{K\text{-}90}K_{J\text{-}90})$ to maintain consistency of units, since I_{ref} is derived from primary voltage and resistance standards using the conventional 1990 values $K_{J\text{-}90}$ and $R_{K\text{-}90}$ for the Josephson and von Klitzing constants, respectively [49]. The normalized difference between e_{90} and the latest SI (CODATA 2014) value of e is $(e_{90} - e)/e_{90} = -8.06 \times 10^{-8}$ [50], so consistency of unit systems is an important consideration as the total measurement uncertainty approaches the 0.1-ppm level. The detailed breakdown of the uncertainty budget for the measurement of I_P is shown in Table I. More information about the precision measurement technique, including a detailed description of each term in Table I, is given in the Supplemental Material [44].

We define the plateau as the region where the fit to the thermal model deviates from the true ef value by less than 0.03 ppm. We show these eight data points on the plateau in the inset of Fig. 4(a). We perform an additional statistical test, detailed in the Supplemental Material [44], to verify that the scatter of the selected data points is consistent with the data being drawn from the same distribution—in other words, that there is no structure on the plateau within our experimental resolution [35]. Averaging these $N_P = 8$

TABLE I. Breakdown of the uncertainty budget for the measurements of the pumped current I_P in Fig. 4. All reported uncertainties are dimensionless 1σ relative uncertainties.

	PL plateau	$B1$ plateau
1. Voltmeter calibration (type A)	0.01 ppm	0.01 ppm
2. Voltmeter linearity (type B)	0.03 ppm	0.03 ppm
3. Voltmeter drift (type B)	0.068 ppm	0.068 ppm
4. 1-GΩ calibration (type B)	0.1 ppm	0.1 ppm
5. 1-GΩ drift (type B)	0.01 ppm	0.01 ppm
6. 1-GΩ calibration (type A)	0.15 ppm	0.07 ppm
7. I_{null} (type B)	0.01 ppm	0.01 ppm
8. I_P (type A)	0.237 ppm	0.229 ppm
Total	0.31 ppm	0.27 ppm

points, we obtain $\Delta I_P = -0.013$ ppm, with a standard deviation of $\sigma(\Delta I_P) = 0.672$ ppm. We take the error of the mean over the data points as the relative statistical (type A) uncertainty for the measurement of the pumped current, $U_A = \sigma(\Delta I_P)/\sqrt{N_P} = 0.237$ ppm. The total relative measurement uncertainty of the pumped current, $U_{\text{total}} = 0.31$ ppm, is given by the root-sum-square of the eight terms listed in Table I, of which U_A is the largest. Thus, the pumped current averaged over the plateau can be expressed as $\Delta I_P = (-0.013 \pm 0.31)$ ppm. To verify the robustness of our device, we also carry out another high-accuracy scan by stepping V_{B1}. In this scan, we find the pumped current averaged over the plateau, shown in the inset of Fig. 4(b), to be $\Delta I_P = (-0.257 \pm 0.27)$ ppm. The deviation of the pumped current from ef is within the measurement uncertainty, and represents the most accurate measurement to date on a silicon SE pump. This work, along with the previous high-accuracy study of silicon devices in the decay-cascade regime [27], indicates that the silicon-based single-electron pump can lead to a more practical and transferable quantum standard of electrical current.

IV. SUMMARY AND OUTLOOK

Despite severe heating in the electron reservoir, the electron pump presented in this work generates a pumped current equal to ef within the ∼0.3 ppm measurement uncertainty at $f = 1$ GHz. Furthermore, fitting the data to a thermal-capture model indicates a theoretical lower bound for the pumping error of 4 ppb at the center of the first current plateau. This suggests that our pump may satisfy the stringent accuracy requirements for a metrological current source [1,6,7]. In addition, the fact that strong magnetic fields or tailored waveform drives are not required for the accurate operation of our pump, could greatly simplify the experimental implementation of the new standard of electrical current.

Note that, by adopting a three-waveform pumping scheme [26], one can potentially reduce the reservoir electron temperature and hence significantly improve the accuracy of our pump in the thermal regime. The three-waveform scheme may reduce the rf amplitude required to pump the electrons and mitigate the drive-induced heating in the source reservoir.

ACKNOWLEDGMENTS

We thank T. Tanttu and K. W. Chan for enlightening discussions and valuable feedback on the manuscript. This work is supported by Australian Research Council (Grants No. DP120104710 and No. DP160104923), the U.S. Army Research Office (W911NF-13-1-0024), the Academy of Finland through its Centre of Excellence Programme (Grant No. 284621), the project EMPIR 15SIB08 e-SI-Amp, and the U.K. Department for Business, Energy and Industrial Strategy. This project has received funding from the European Metrology Programme for Innovation and Research (EMPIR) programme cofinanced by the Participating States and from the European Union's Horizon 2020 research and innovation programme. We acknowledge the Australian National Fabrication Facility for the support in device manufacturing. A. R. acknowledges support from the European Union's Horizon 2020 research and innovation programme under the Marie Sklodowska-Curie grant agreement No. 654712 (SINHOPSI).

[1] Jukka P. Pekola, Olli-Pentti Saira, Ville F. Maisi, Antti Kemppinen, Mikko Möttönen, Yuri A. Pashkin, and Dmitri V. Averin, Single-electron current sources: Toward a refined definition of the ampere, Rev. Mod. Phys. **85**, 1421 (2013).

[2] Bernd Kaestner and Vyacheslavs Kashcheyevs, Non-adiabatic quantized charge pumping with tunable-barrier quantum dots: A review of current progress, Rep. Prog. Phys. **78**, 103901 (2015).

[3] M. Kataoka, N. Johnson, C. Emary, P. See, J. P. Griffiths, G. A. C. Jones, I. Farrer, D. A. Ritchie, M. Pepper, and T. J. B. M. Janssen, Time-of-Flight Measurements of Single-Electron Wave Packets in Quantum Hall Edge States, Phys. Rev. Lett. **116**, 126803 (2016).

[4] J. D. Fletcher, P. See, H. Howe, M. Pepper, S. P. Giblin, J. P. Griffiths, G. A. C. Jones, I. Farrer, D. A. Ritchie, T. J. B. M. Janssen, and M. Kataoka, Clock-Controlled Emission of Single-Electron Wave Packets in a Solid-State Circuit, Phys. Rev. Lett. **111**, 216807 (2013).

[5] Niels Ubbelohde, Frank Hohls, Vyacheslavs Kashcheyevs, Timo Wagner, Lukas Fricke, Bernd Kästner, Klaus Pierz, Hans W. Schumacher, and Rolf J. Haug, Partitioning of on-demand electron pairs, Nat. Nanotechnol. **10**, 46 (2015).

[6] F. Piquemal and G. Genevés, Argument for a direct realization of the quantum metrological triangle, Metrologia **37**, 207 (2000).

[7] Mark W. Keller, John M. Martinis, Neil M. Zimmerman, and Andrew H. Steinbach, Accuracy of electron counting using a 7-junction electron pump, Appl. Phys. Lett. **69**, 1804 (1996).

[8] Mark W. Keller, Ali L. Eichenberger, John M. Martinis, and Neil M. Zimmerman, A capacitance standard based on counting electrons, Science **285**, 1706 (1999).

[9] J. M. Shilton, V. I. Talyanskii, M. Pepper, D. A. Ritchie, J. E. F. Frost, C. J. B. Ford, C. G. Smith, and G. A. C. Jones, High-frequency single-electron transport in a quasi-one-dimensional GaAs channel induced by surface acoustic waves, J. Phys. Condens. Matter **8**, L531 (1996).

[10] V. I. Talyanskii, J. M. Shilton, M. Pepper, C. G. Smith, C. J. B. Ford, E. H. Linfield, D. A. Ritchie, and G. A. C. Jones, Single-electron transport in a one-dimensional channel by high-frequency surface acoustic waves, Phys. Rev. B **56**, 15180 (1997).

[11] Antti O. Niskanen, Jani M. Kivioja, Heikki Seppä, and Jukka P. Pekola, Evidence of cooper-pair pumping with

combined flux and voltage control, Phys. Rev. B **71**, 012513 (2005).
[12] Juha J. Vartiainen, Mikko Möttönen, Jukka P. Pekola, and Antti Kemppinen, Nanoampere pumping of cooper pairs, Appl. Phys. Lett. **90**, 082102 (2007).
[13] Mikko Möttönen, Juha J. Vartiainen, and Jukka P. Pekola, Experimental Determination of the Berry Phase in a Superconducting Charge Pump, Phys. Rev. Lett. **100**, 177201 (2008).
[14] Jukka P. Pekola, Juha J. Vartiainen, Mikko Möttönen, Olli-Pentti Saira, Matthias Meschke, and Dmitri V. Averin, Hybrid single-electron transistor as a source of quantized electric current, Nat. Phys. **4**, 120 (2008).
[15] M. D. Blumenthal, B. Kaestner, L. Li, S. Giblin, T. J. B. M. Janssen, M. Pepper, D. Anderson, G. Jones, and D. A. Ritchie, Gigahertz quantized charge pumping, Nat. Phys. **3**, 343 (2007).
[16] X. Jehl *et al.*, Hybrid Metal-Semiconductor Electron Pump for Quantum Metrology, Phys. Rev. X **3**, 021012 (2013).
[17] S. P. Giblin, M. Kataoka, J. D. Fletcher, P. See, T. J. B. M. Janssen, J. P. Griffiths, G. A. C. Jones, I. Farrer, and D. A. Ritchie, Towards a quantum representation of the ampere using single electron pumps, Nat. Commun. **3**, 930 (2012).
[18] Friederike Stein *et al.*, Validation of a quantized-current source with 0.2 ppm uncertainty, Appl. Phys. Lett. **107**, 103501 (2015).
[19] S. P. Giblin, P. See, A. Petrie, T. J. B. M. Janssen, I. Farrer, J. P. Griffiths, G. A. C. Jones, D. A. Ritchie, and M. Kataoka, High-resolution error detection in the capture process of a single-electron pump, Appl. Phys. Lett. **108**, 023502 (2016).
[20] M. R. Connolly, K. L. Chiu, S. P. Giblin, M. Kataoka, J. D. Fletcher, C. Chua, J. P. Griffiths, G. A. C. Jones, V. I. Fal'Ko, C. G. Smith, and T. J. B. M. Janssen, Gigahertz quantized charge pumping in graphene quantum dots, Nat. Nanotechnol. **8**, 417 (2013).
[21] Akira Fujiwara, Neil M. Zimmerman, Yukinori Ono, and Yasuo Takahashi, Current quantization due to single-electron transfer in Si-wire charge-coupled devices, Appl. Phys. Lett. **84**, 1323 (2004).
[22] Akira Fujiwara, Katsuhiko Nishiguchi, and Yukinori Ono, Nanoampere charge pump by single-electron ratchet using silicon nanowire metal-oxide-semiconductor field-effect transistor, Appl. Phys. Lett. **92**, 042102 (2008).
[23] Yukinori Ono and Yasuo Takahashi, Electron pump by a combined single-electron/field-effect-transistor structure, Appl. Phys. Lett. **82**, 1221 (2003).
[24] K. W. Chan, M. Möttönen, A. Kemppinen, N. S. Lai, K. Y. Tan, W. H. Lim, and A. S. Dzurak, Single-electron shuttle based on a silicon quantum dot, Appl. Phys. Lett. **98**, 212103 (2011).
[25] Alessandro Rossi, Tuomo Tanttu, Kuan Yen Tan, Ilkka Iisakka, Ruichen Zhao, Kok Wai Chan, Giuseppe C. Tettamanzi, Sven Rogge, Andrew S. Dzurak, and Mikko Möttönen, An accurate single-electron pump based on a highly tunable silicon quantum dot, Nano Lett. **14**, 3405 (2014).
[26] Tuomo Tanttu, Alessandro Rossi, Kuan Yen Tan, Akseli Mäkinen, Kok Wai Chan, Andrew S. Dzurak, and Mikko Möttönen, Three-waveform bidirectional pumping of single electrons with a silicon quantum dot, Sci. Rep. **6**, 36381 (2016).
[27] Gento Yamahata, Stephen P. Giblin, Masaya Kataoka, Takeshi Karasawa, and Akira Fujiwara, Gigahertz single-electron pumping in silicon with an accuracy better than 9.2 parts in 107, Appl. Phys. Lett. **109**, 013101 (2016).
[28] Gento Yamahata, Stephen P Giblin, Masaya Kataoka, Takeshi Karasawa, and Akira Fujiwara, High-accuracy current generation in the nanoampere regime from a silicon single-trap electron pump, Sci. Rep. **7**, 45137 (2017).
[29] Gento Yamahata, Katsuhiko Nishiguchi, and Akira Fujiwara, Gigahertz single-trap electron pumps in silicon, Nat. Commun. **5**, 5038 (2014).
[30] G. C. Tettamanzi, Romain Wacquez, and S. Rogge, Charge pumping through a single donor atom, New J. Phys. **16**, 063036 (2014).
[31] G. P. Lansbergen, Y. Ono, and A. Fujiwara, Donor-based single electron pumps with tunable donor binding energy, Nano Lett. **12**, 763 (2012).
[32] B. Roche, R.-P. Riwar, B. Voisin, E. Dupont-Ferrier, R. Wacquez, M. Vinet, M. Sanquer, J. Splettstoesser, and X. Jehl, A two-atom electron pump, Nat. Commun. **4**, 1581 (2013).
[33] Myung-Ho Bae, Ye-Hwan Ahn, Minky Seo, Yunchul Chung, J. D. Fletcher, S. P. Giblin, M. Kataoka, and Nam Kim, Precision measurement of a potential-profile tunable single-electron pump, Metrologia **52**, 195 (2015).
[34] F. Stein, H. Scherer, T. Gerster, R. Behr, M. Götz, E. Pesel, C. Leicht, N. Ubbelohde, T. Weimann, K. Pierz *et al.*, Robustness of single-electron pumps at sub-ppm current accuracy level, Metrologia **54**, S1 (2017).
[35] S. P. Giblin, M. H. Bae, N. Kim, Ye-Hwan Ahn, and M. Kataoka, Robust operation of a GaAs tunable barrier electron pump, Metrologia **54**, 299 (2017).
[36] Vyacheslavs Kashcheyevs and Bernd Kaestner, Universal Decay Cascade Model for Dynamic Quantum Dot Initialization, Phys. Rev. Lett. **104**, 186805 (2010).
[37] Gento Yamahata, Katsuhiko Nishiguchi, and Akira Fujiwara, Accuracy evaluation and mechanism crossover of single-electron transfer in Si tunable-barrier turnstiles, Phys. Rev. B **89**, 165302 (2014).
[38] Vyacheslavs Kashcheyevs and Janis Timoshenko, Modeling of a tunable-barrier non-adiabatic electron pump beyond the decay cascade model, in *Proceedings of the Conference on Precision Electromagnetic Measurements (CPEM 2014)* (IEEE, New York, 2014), pp. 536–537.
[39] Lukas Fricke, Michael Wulf, Bernd Kaestner, Vyacheslavs Kashcheyevs, Janis Timoshenko, Pavel Nazarov, Frank Hohls, Philipp Mirovsky, Brigitte Mackrodt, Ralf Dolata, Thomas Weimann, Klaus Pierz, and Hans W. Schumacher, Counting Statistics for Electron Capture in a Dynamic Quantum Dot, Phys. Rev. Lett. **110**, 126803 (2013).
[40] Susan J. Angus, Andrew J. Ferguson, Andrew S. Dzurak, and Robert G. Clark, Gate-defined quantum dots in intrinsic silicon, Nano Lett. **7**, 2051 (2007).
[41] Alessandro Rossi, Tuomo Tanttu, Fay E. Hudson, Yuxin Sun, Mikko Möttönen, and Andrew S. Dzurak, Silicon metal-oxide-semiconductor quantum dots for single-electron pumping, J. Vis. Exp. **100**, e52852 (2015).

[42] Mark E. Law and Stephen M. Cea, Continuum based modeling of silicon integrated circuit processing: An object oriented approach, Comput. Mater. Sci. **12**, 289 (1998).

[43] H. Pothier, P. Lafarge, C. Urbina, D. Esteve, and M. H. Devoret, Single-electron pump based on charging effects, Europhys. Lett. **17**, 249 (1992).

[44] See Supplemental Material at http://link.aps.org/supplemental/10.1103/PhysRevApplied.8.044021 for more information about the addition energy extraction, TCAD simulation, and as well as the precision measurement technique.

[45] M. Kataoka, J. D. Fletcher, P. See, S. P. Giblin, T. J. B. M. Janssen, J. P. Griffiths, G. A. C. Jones, I. Farrer, and D. A. Ritchie, Tunable Nonadiabatic Excitation in a Single-Electron Quantum Dot, Phys. Rev. Lett. **106**, 126801 (2011).

[46] J. D. Fletcher, M. Kataoka, S. P. Giblin, Sunghun Park, H.-S. Sim, P. See, D. A. Ritchie, J. P. Griffiths, G. A. C. Jones, H. E. Beere, and T. J. B. M. Janssen, Stabilization of single-electron pumps by high magnetic fields, Phys. Rev. B **86**, 155311 (2012).

[47] S. P. Giblin (to be published).

[48] Dietmar Drung, Christian Krause, Stephen P. Giblin, Sophie Djordjevic, Francois Piquemal, Olivier Séron, Florentin Rengnez, Martin Götz, Eckart Pesel, and Hansjörg Scherer, Validation of the ultrastable low-noise current amplifier as travelling standard for small direct currents, Metrologia **52**, 756 (2015).

[49] N. M. Zimmerman, A primer on electrical units in the systeme international, Am. J. Phys. **66**, 324 (1998).

[50] Peter J. Mohr, David B. Newell, and Barry N. Taylor, Codata recommended values of the fundamental physical constants: 2014, J. Phys. Chem. Ref. Data **45**, 043102 (2016), reference on p. 65.